

LONG-WAVELENGTH VORTEX MOTION INDUCED BY FREE-STREAM TURBULENCE

S. Bailey and B. Estejab

Department of Mechanical Engineering,
University of Kentucky
Lexington, KY, 40506, USA
email: scbailey@engr.uky.edu

M. Robert and S.Tavoularis

Department of Mechanical Engineering
University of Ottawa
Ottawa, ON, K1N 6N5, Canada
email: stavros.tavoularis@uottawa.ca

ABSTRACT

This study further examines experimentally the motion of an isolated vortex immersed in grid-generated free-stream turbulence. Using a novel analytical procedure, we determined approximately the time history of the vortex axis position from velocity vectors at two locations measured simultaneously with the use of hot-wire anemometry. We identified a long-wavelength, organized, helical motion of the vortex axis, which is present in both low-turbulence and high-turbulence streams, thus pointing to a universal instability mechanism. Free-stream turbulence appears to intensify this instability, while simultaneously enhancing the stochastic motion of the vortex axis.

INTRODUCTION

The study of wing tip vortices has been motivated by the potential hazards they pose to aviation. It is well known that wing tip vortices in the atmosphere decay very slowly. It is also known that their decay rate is enhanced by atmospheric turbulence, however, the vorticity dissipation mechanisms have not been adequately understood and it is not currently possible to predict accurately the vortex decay rate.

Spalart (1998) describes two potential modes for decay of trailing vortices: a) predictable decay, whereby the vortex circulation decreases monotonically with time; and b) stochastic collapse, whereby the vortex circulation remains relatively constant in time until the occurrence of a dramatic event which rapidly dissipates the circulation; such events include vortex linking or destruction by external turbulence. van Jaarsveld et al. (2011) recently conducted a series of wind tunnel measurements, which supported the stochastic collapse model, observing evidence of both long-wave Crow (1970) instabilities and direct destruction of the vortices by external turbulence. Crow and Bate (1976) proposed that direct destruction of multiple vortices will occur when the

amplitudes of motions of individual vortices caused by external turbulence exceed the vortex spacing. To predict the onset of cooperative instabilities or destruction of the vortex pairs due to external turbulence, it would be necessary to characterize the unsteady deflections of vortices within turbulent surroundings.

Transverse motion of a vortex, commonly referred to as wandering or meandering, has been well documented in wind tunnel studies of trailing vortices (see Devenport et al., 1996, for example) and is often attributed to unsteadiness in wind tunnel flow conditions. In the presence of external turbulence, the vortex motion is significantly amplified (Heyes et. al. 2004; Bailey and Tavoularis, 2008; Beresh et. al. 2010). For full-scale aircraft vortices in atmospheric turbulence, vortex wandering could potentially initiate stochastic collapse of vortex pairs through initiation and amplification of cooperative instabilities or vorticity annihilation through vortex merging.

Despite its potential importance, vortex wandering in turbulent flows has not been characterized sufficiently, partly because of difficulties in performing accurate time-resolving measurements of the velocity field of a wandering vortex. Several studies, including Devenport et al. (1996), Heyes et. al. (2004), Bailey and Tavoularis (2008), Beresh et. al. (2010) and van Jaarsveld et al. (2011), note that in the vortex cross-plane the vortex position appears to have a nearly Gaussian probability distribution. These studies have not resolved the streamwise waveform of vortex motions, nor documented its dependence on free-stream turbulence, although they often inferred that such motions have long wavelengths. Takahashi et al. (2005) suggested that secondary vortical structures surrounding the primary vortex excite vortex bending and axisymmetric waves in the vortex, which could be interpreted as vortex wandering.

The objective of the current study is to investigate experimentally the time-dependent motion of an isolated

vortex immersed in free-stream turbulence, focusing on the wavelengths of the motion. This work is a continuation of previous studies of vortices embedded in turbulence, which reported time averaged (Bailey et al., 2006) and conditionally averaged velocity measurements (Bailey and Tavoularis, 2008), and analysed these results to elucidate the effect of free-stream turbulence on properties of an isolated vortex. Like the previous studies, the present work considers the statistically simple case of nearly isotropic, grid-generated turbulence with different turbulence intensities and length scales. Of primary concern was to investigate whether vortex meandering is purely random, as speculated in the literature, or if it has a quasi-periodic, organized structure.

EXPERIMENT DESCRIPTION

Two distinct sets of experiments have been conducted, one in a wind tunnel and another in a water channel. In both cases the vortex was generated using a square-tipped, NACA 0012 airfoil, with a chord $c = 178$ mm and placed at an angle of attack of 5° . The wing aspect ratio was 2.9 for the wind tunnel tests and 1.7 for the water channel tests. The Reynolds numbers based on the chord were, respectively, 2.4×10^5 and 2.3×10^4 .

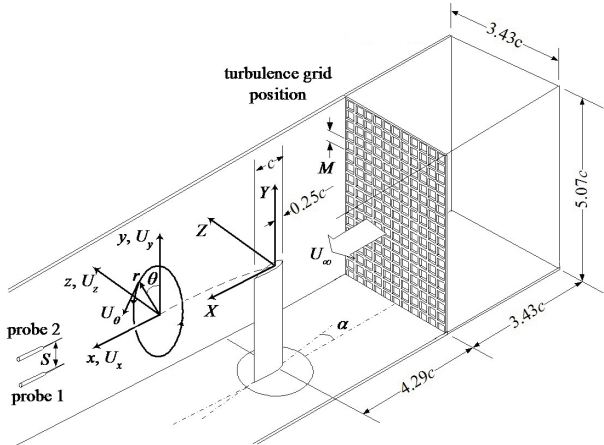


Figure 1. Schematic diagram showing the experimental setup in the wind tunnel and relevant nomenclature.

Free-stream turbulence in either case was generated by one of two grids, both with a solidity of 0.44 and square perforations with mesh sizes of $M = 50.8$ mm ("large-grid" case) and $M = 25.4$ mm ("small-grid" case). At $X/c = 0$, the turbulence intensity was approximately 5% and 2.5% for the large-grid and small-grid cases, respectively. Following well known grid turbulence patterns, the turbulence kinetic energy decayed with distance from the grid, whereas the integral length scale grew. A detailed documentation of the free-stream turbulence in the wind tunnel has been reported by Bailey and Tavoularis (2008).

The wind-tunnel experimental arrangement is sketched in Fig. 1, which also shows the definition of the wing-fixed $[X, Y, Z]$ and mean vortex-trajectory fixed $[x, y, z]$ Cartesian coordinate systems used here. In the wind tunnel, two custom-built, four-sensor, modified Kovasznay-type hot-wire probes were used to measure the instantaneous, local velocity vector. The measurement volume of either probe had dimensions approximately equal to $0.5 \times 0.5 \times 0.5$ mm³. One of the probes was fixed at the mean location of the vortex axis and the other one was mounted on a manually operated traverse so that it could be separated from the fixed probe in the direction of the wing span by a distance S in the range from 7.1 to 27.6 mm. Velocity data from both four-sensor probes were digitized simultaneously at a rate of 30 kHz and recorded over 180 s.

In the water channel, 1000 instantaneous velocity maps were collected at a rate of 5 Hz for each case, using a planar PIV system in the Scheimpflug configuration.

IDENTIFICATION OF VORTEX POSITION

Wind Tunnel Experiment

Previous analysis of the wind tunnel results by Bailey and Tavoularis (2008) has reconstructed the velocity field of the vortex in a frame of reference wandering with the vortex, as well as providing probability density functions of vortex position. The goal of the present analysis is to reconstruct the temporal history of the vortex axis position, thus allowing a detailed examination of the vortex motion induced by the turbulence. To determine the vortex position from the two-point velocity measurements, we devised an algorithm which takes into consideration the three-dimensional velocity time series from both probes as well as the velocity profiles measured by Bailey and Tavoularis (2008); this algorithm provides a time series of the most probable vortex position $[y_v(t), z_v(t)]$ at each instant in time.

The analysis proceeds as follows. First, a velocity field $[U'_y(y, z), U'_z(y, z)]$ was created using the wandering-free vortex velocity profile determined by Bailey and Tavoularis (2008) for the corresponding local free-stream conditions and streamwise distance from the wing. Let the velocities measured by the probes at time t be $[U_y(0, 0, t), U_z(0, 0, t)]$ and $[U_y(0, S, t), U_z(0, S, t)]$. Note, only results with $S = 5.1$ mm have been processed to date. Next, a first guess of the location of the vortex axis relative to the mean axis location was made as $[y', z']$. Using this position, an error parameter was calculated as

$$e = [U'_y(-y', -z') - U_y(0, 0, t)]^2 + [U'_z(-y', -z') - U_z(0, 0, t)]^2 + [U'_y(-y', -z' + S) - U_y(0, S, t)]^2 + [U'_z(-y', -z' + S) - U_z(0, S, t)]^2 \quad (1)$$

The assumed vortex position $[y', z']$ was then iterated through a range of possible positions using a rectangular grid with spacing $\Delta y'$ and $\Delta z' = 0.006$ mm. Once error parameter values e were calculated for all $[y', z']$ positions, the location $[y', z']$ with the minimum value of e was identified as the most probable location of the vortex at time t . The entire process was then repeated for the next set of points in the velocity time series, producing a time-series of vortex position, $[y_v(t), z_v(t)]$.

After a first data processing pass, occasional events could be observed in the vortex trajectory which entailed large excursions in vortex position, following which the vortex almost immediately returned to a position close to the previous one. These instances were identified as probable mis-identification events. To quantify and remove these events, an automated outlier detection scheme was employed, which located instances at which the magnitude of the vortex velocity deviated from the mean (which was approximately zero) by more than 3 standard deviations. The position values at these instances, accounting for less than 0.1% of the entire time series length, were discarded and replaced by values estimated by interpolation.

Water Tunnel Experiment

The vortex position in the water tunnel experiments was determined as the location of maximal vorticity in the corresponding plane of measurement. The temporal resolution of the PIV system was insufficient to describe the temporal history of the vortex axis position. Although, at first glance, PIV measurements appeared to resolve the low-frequency content, corresponding to wavelengths longer than about one wing chord, in the absence of a low-pass filtering process, such measurements would be contaminated by aliasing and so they were presently used only to determine the wandering amplitude.

WANDERING AMPLITUDE

As representative results, Figs. 2a-c show fragments, 1 ms long, of the time-series of vortex axis position [$y_v(t)$, $z_v(t)$] at $X/c = 9.75$. In each case, the vortex is seen to follow an apparently stochastic motion about the mean axis located at [0,0]. The corresponding joint probability density functions (JPDF) of the vortex position over the entire time series length, plotted in Figs. 2d-f, may be fitted fairly well by bivariate normal JPDF. Within the considerable experimental uncertainty of the present approach, Fig. 3 further shows that the probability density functions (PDF) of the vortex position in the y and z directions are approximately Gaussian, in agreement with observations in the literature (Devenport et al., 1996; Heyes et al., 2004; Bailey and Tavoularis, 2008; Beresh et al., 2010; van Jaarsveld et al., 2011). Consequently, the amplitude of wandering can be effectively described by the standard deviations of y_v and z_v , denoted by σ_y and σ_z , respectively. As shown in Fig. 4, the wandering amplitude increases with both streamwise distance from the wing and free-stream turbulence intensity. Further, the amplitude is approximately the same in both y and z directions. The agreement between the wandering amplitudes estimated using the current analysis and the ones reported by Bailey and Tavoularis (2008) for the no-grid and small-grid cases is excellent. The differences for the large-grid case are somewhat large, but still within the estimated uncertainty limits. Therefore, we may conclude that the present analysis successfully captures the vortex motion.

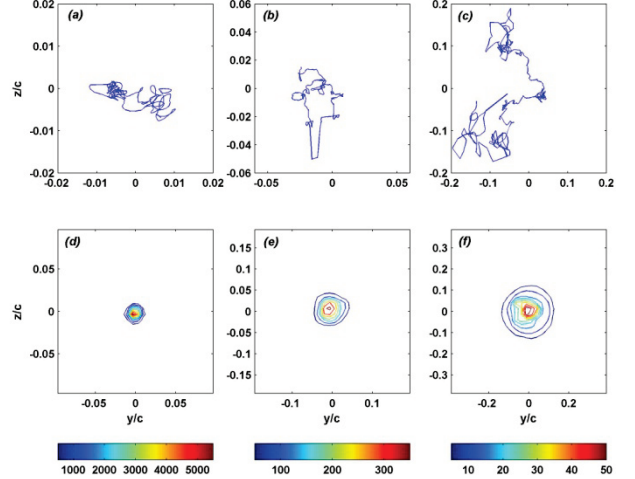


Figure 2. Trajectory of vortex axis for the (a) no-grid, (b) small-grid and (c) large-grid cases at $X/c = 9.75$ during 1 ms. Corresponding JPDFs of vortex position for the (d) no-grid, (e) small-grid and (f) large-grid cases. The shown ranges of axes increase from left to right.

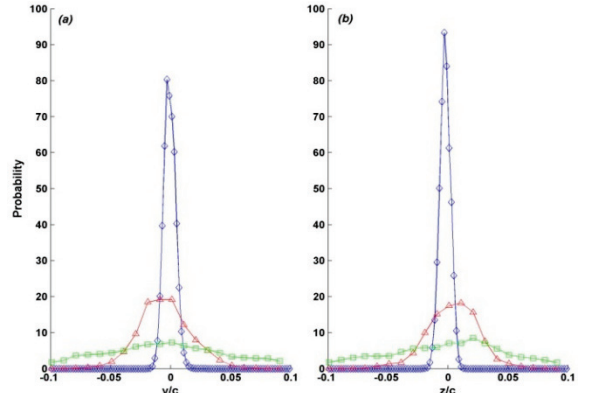


Figure 3. Probability density functions of vortex axis position in (a) y -direction and (b) z -direction at $X/c = 9.75$ for the no grid (blue), small grid (red) and large grid (green) cases.

The PIV results, as shown in figure 5, are compatible with the wind tunnel results, if one takes into consideration the differences in Reynolds numbers and free-stream turbulence levels between the two experiments. The most notable difference is that the amplitudes of wandering for the no-grid and small-grid cases are much higher in the water tunnel tests; this may be attributed to the observed presence of higher background disturbances in the water tunnel or, alternatively, to an increased susceptibility of the vortex to wandering at lower Reynolds numbers.

FREQUENCY ANALYSIS

Vortex wandering motions have previously been either directly determined from PIV studies (Heyes et al., 2004; Beresh et al., 2010; van Jaarsveld et al., 2011) or indirectly

inferred from velocity time series (Devenport et al., 1996; Bailey and Tavoularis, 2008). However, these methods are limited in their ability to examine the temporal variation of vortex position. With the current analysis of the wind tunnel results, we are now able, for the first time, to determine the frequency content of the vortex wandering.

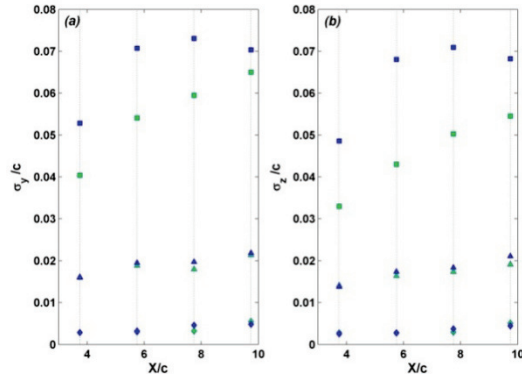


Figure 4. Wandering amplitude in (a) y -direction and (b) z -direction from the wind tunnel study; present results are in blue and those by Bailey and Tavoularis (2008) are in green; no-grid (\diamond); small-grid (\triangle) and large-grid (\square) cases.

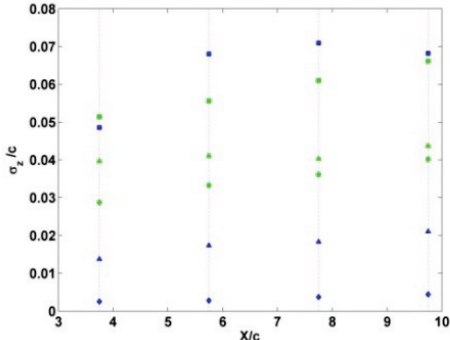


Figure 5. Comparison of estimated standard deviations of vortex position (wandering amplitude) in the z -direction from water tunnel PIV measurements (green symbols) with those by the present analysis (blue symbols); no-grid (\diamond), small-grid (\triangle) and large-grid (\square) cases.

Frequency spectra $\Phi_{yy}(f)$ of y_v , are presented in Figs. 6a-c for the three cases examined; frequency spectra for z_v were virtually identical to the corresponding y_v spectra. The spectra are presented in pre-multiplied form $f\Phi_{yy}(f)$, which provides a better visual indication of the frequency ranges of the energetic wavelengths of the vortex motion. In conformity with the results presented in Fig. 4, the amplitude of the frequency spectrum increases with X/c in all cases.

For the no-grid case (Fig. 6a), there are three noticeable broadband peaks (marked by arrows) evident in the spectra for all cases, indicating three dominant wavelengths of wandering motion. Near the wing, at $X/c = 3.75$, the power content of the

lowest frequency (longest wavelength) motion is comparable to the power content of the two short-wavelength motions. However, as the vortex evolves downstream, the power of the long-wavelength motion grows, whereas the powers of the two shorter wavelength motions decay.

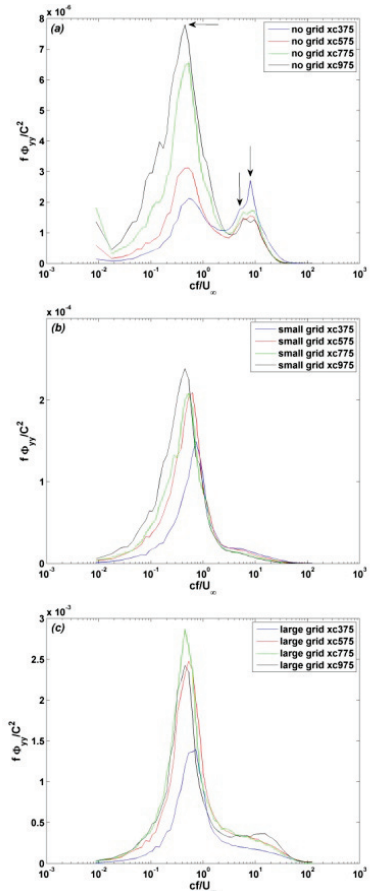


Figure 6. Pre-multiplied frequency spectra of y_v for (a) no-grid, (b) small-grid and (c) large-grid cases.

In contrast with the no-grid case, only a single peak in the frequency spectrum is evident for each of the two turbulent free stream cases, which show relatively weak broadband motions at higher frequencies. As with the no-grid case, the long-wavelength motion increases in power with streamwise distance, indicating that the wandering amplitude is driven mainly by this low frequency motion.

The wavelengths of the dominant low frequency motions in the y and z directions can be estimated from the frequencies of the peaks in the frequency spectra and the convection velocity, approximated by the free-stream velocity U_∞ . The results are presented in Fig. 7, which shows that the wavelength of the low-frequency/long-wavelength motion increases gradually with streamwise distance from the wing for all cases and is approximately the same in both the y and z

directions. The most striking observation that can be made from Figs. 7a-b is that, unlike the wandering amplitude, the dominant wandering wavelength appears to be independent of free-stream turbulence intensity (within the expected uncertainty of peak frequency identification). This indicates that the free-stream turbulence only serves to excite existing instability modes and does not generate new modes of motion.

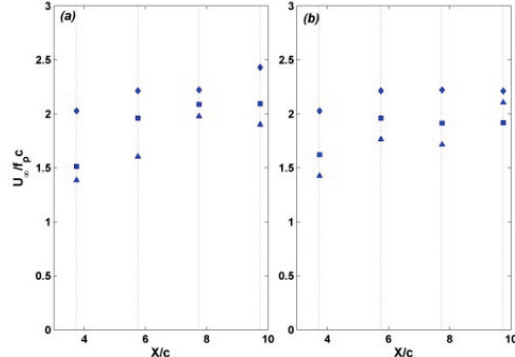


Figure 7. Estimated wavelengths corresponding to low-frequency spectral peaks for (a) y -direction and (b) z -direction; no-grid (\diamond), small-grid (\triangle) and large-grid (\square) cases.

The short-wavelength modes observed for the no-grid case showed no appreciable dependence on streamwise distance. In the presence of external, broadband turbulence, such motions were not clearly discernible.

The bi-normality of the JPDFs (Fig. 2), the normality of the PDFs (Fig. 3), and the wideband nature of spectral peaks (Fig. 6) are all compatible with both stochastic and quasi-periodic vortex wandering. However, strong evidence of organization within the wandering is provided by the presence of strong peaks in cross-correlations of y_v and z_v , shown in Fig. 8. Peaks are visible in all cases, but their amplitudes increase with increasing free-stream turbulence and decrease with distance from the grid. In all cases, the main central maximum is positive and is flanked by weaker minima, which, at least for the grid-turbulence cases, are all negative. Correlation between wanderings in the two directions is unmistakable evidence of periodic, organized motion. The period of this motion is reflected in the temporal spacing between the negative peaks in the cross-correlation, and corresponds to the wavelengths shown in Fig. 7.

Focusing on the two cases with free-stream turbulence, it is evident that the peaks in the cross-correlations occur at negative time lags $\Delta\tau$, as shown more clearly in Fig. 9. The magnitude of the time lag increases with increasing distance from the wing, but seems to be insensitive to the turbulence intensity. For the no-grid case, determining the time lag was difficult because of the weak correlation, however, for $X/c = 3.75$ and 5.75 , it appears that the time lag is comparable to those for the cases with free-stream turbulence.

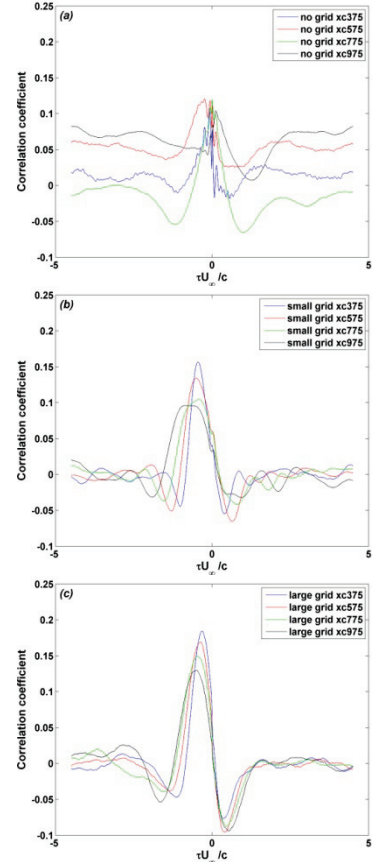


Figure 8. Cross-correlation of y_v and z_v , calculated at different X/c positions for the (a) no-grid, (b) small-grid and (c) large-grid cases.

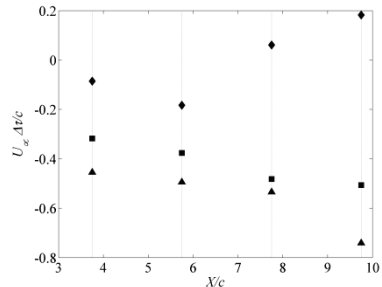


Figure 9. Time lag observed in cross-correlation of y_v and z_v for the no-grid (\diamond), small-grid (\triangle) and large-grid (\square) cases.

Combining the wavelength results shown in Fig. 7 with the cross-correlation time lags shown in Fig. 9, one may roughly estimate a phase angle of approximately -70° between y_v and z_v . This, together with the evidence of weak periodicity and virtually identical wavelengths in the y and z directions, point to a helical pattern of long-wavelength, organized, wandering motion. The sense of rotation of this helix is the same as that of the primary vortex.

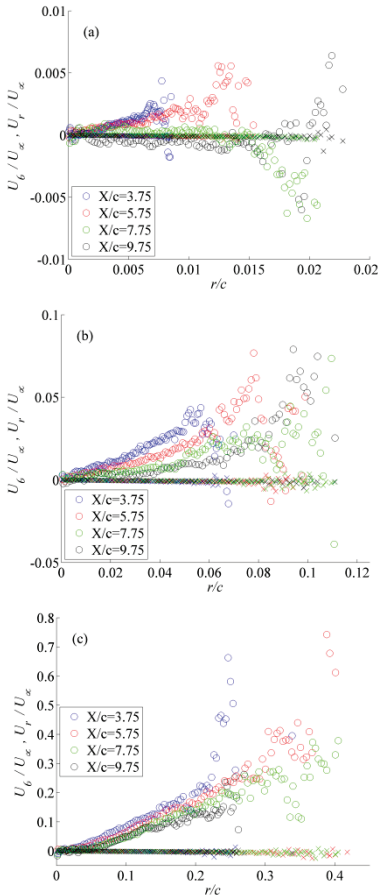


Figure 10. Average velocity of the vortex motion in (○) circumferential and (×) radial directions as a function of radial position from mean vortex center for (a) no-grid case, (b) small-grid case and (c) large-grid case.

To study this long wavelength motion in detail, the radial and circumferential components of the translational velocity of the vortex axis relative to the mean axis were determined from finite differencing the y_v and z_v time series after low-pass filtering with a cut-off at $f_c/U_\infty = 1$. The radial dependence relative to the mean vortex axis of both the mean radial U_r and circumferential U_θ components of the translation velocity are shown in Fig. 10 for all cases. The results show that, whereas $U_r \approx 0$ everywhere, there is a non-zero U_θ , consistent with a helical vortex motion. U_θ is found to exhibit characteristics of solid-body rotation, increasing linearly with radial distance, until the outer edge of the wandering extent, where U_θ can be seen to decrease, notably for the small-grid case.

Thus, this instability process may also be viewed as signifying that the primary vortex is subject to wandering by being embedded within a much weaker surrounding vortex. This notion might explain the observation by Bailey and Tavoularis (2008) that the primary vortex circulation decreased downstream for the turbulence grid cases; it seems possible that vorticity is being transferred from the primary vortex to the large-scale wandering.

CONCLUSIONS

An analysis of two-point, multi-component velocity measurements was conducted for a trailing vortex immersed in free-stream turbulence to determine the temporal variation of the vortex axis position. The results indicate that, although the vortex motion is largely stochastic, it also has an organized component in the form of a helical motion with a long wavelength. Transfer of vorticity from the vortex into the helical motion could explain the loss of circulation observed in previous studies. The wavelength of this motion is insensitive to free-stream turbulence, but the amplitude increases with turbulence intensity. Therefore, it appears that the free-stream turbulence only serves to enhance an existing mode of motion without generating additional organized modes of motion. As expected, increased turbulence intensifies vortex wandering across a broadband frequency range. Multiple power spectral peaks of vortex motion were observed in the case without free-stream turbulence. The higher frequency motions rapidly decayed downstream of the wing, whereas the long-wavelength motion became more dominant.

REFERENCES

- Bailey, S. C. C. and Tavoularis, S., 2008, "Measurements of the velocity field of a wing-tip vortex, wandering in grid turbulence", *Journal of Fluid Mechanics*, Vol. 601, pp. 281-315.
- Bailey, S. C. C., Tavoularis, S. and Lee, B. H. K., 2006, "Effects of freestream turbulence on wing-tip vortex formation and near field", *Journal of Aircraft*, Vol. 43, No. 5, pp. 1282-1291.
- Beresh, S. J., Henfling, J. F. and Spillers, R. W., 2010, "Meander of a fin trailing vortex and the origin of its turbulence", *Experiments in Fluids*, Vol. 49, pp. 599-611.
- Crow, S. C., 1970, "Stability theory for a pair of trailing vortices", *AIAA Journal*, Vol. 8, pp. 2172-2179.
- Crow, S. C. and Bate, E. R., 1976, "Lifespan of trailing vortices in a turbulent atmosphere", *Journal of Aircraft*, Vol. 13, pp. 476-482.
- Devenport, W. J., Rife, M. C., Liapis, S. I. and Follin, G. J., 1996, "The structure and development of a wing-tip vortex", *Journal of Fluid Mechanics*, Vol. 312, pp. 67-106.
- Heyes, A. L., Jones, R. F., Smith, D. A. R., 2004, "Wandering of wing-tip vortices." *Proceedings of the 12th International Symposium on Applications of Laser Techniques to Fluid Mechanics*, Lisbon, Portugal, Paper 35-3.
- van Jaarsveld, J. P. J., Holten, A. P. C., Elsenaar, A. and Trieling, R. R. and van Heijst, G. J. F., 2011, "An experimental study of the effect of external turbulence on the decay of a single vortex and vortex pair", *Journal of Fluid Mechanics*, Vol. 670, pp. 214-239.
- Spalart, P., 1998, "Airplane trailing vortices", *Annual Reviews in Fluid Mechanics*, Vol. 30, pp. 107-138.
- Takahashi, N., Ishii, H. and Miyazaki, T., 2005, "The influence of turbulence on a columnar vortex", *Physics of Fluids*, Vol. 17, 035105.